Ultrasound-mediated destruction of contrast microbubbles used for medical imaging and drug delivery

Dhiman Chatterjee
Mechanical Engineering, University of Delaware, Newark, Delaware 19716
and Department of Mechanical Engineering, Indian Institute of Technology, Madras (IITM), Chennai 600 036, India

Pankaj Jain and Kausik Sarkar[a)]
Mechanical Engineering, University of Delaware, Newark, Delaware 19716

(Received 18 November 2004; accepted 7 July 2005; published online 3 October 2005)

Micron-size bubbles encapsulated by a stabilizing layer of surface-active materials are used in medical ultrasound imaging and drug delivery. Their destruction stimulated by ultrasound *in vivo* plays a critical role in both applications. We investigate the destruction process of microbubbles in a commercially available contrast agent by measuring the attenuation of ultrasound through it. The measurement is performed with single-cycle bursts from an unfocused transducer (with a center frequency of 5 MHz) for varying pressure amplitudes at 50-, 100-, and 200-Hz pulse repetition frequencies (PRF) with duty cycles 0.001%, 0.002%, and 0.004%, respectively. At low excitation, the attenuation is found to increase with time. With increased excitation level, the attenuation level decreases with time, indicating destruction of microbubbles. There is a critical pressure amplitude ($\sim$1.2 MPa) for all three PRFs, below which there is no significant bubble destruction. Above the critical pressure amplitudes the rate of destruction depends on excitation levels. But at high-pressure amplitudes the destruction becomes independent of excitation pressure amplitude. The results are interpreted to identify two different mechanisms of bubble destruction by its signature in attenuation, namely, slow dissolution by diffusion and catastrophic shell rupture. The different modes are discussed in detail with their implications in medical applications. © *2005 American Institute of Physics*. [DOI: 10.1063/1.2011468]

I. INTRODUCTION

Ultrasound imaging is the safest and the least expensive modality of medical imaging. The quality of an ultrasound image depends on the difference in reflection of ultrasound from different tissues. A significant improvement of ultrasound blood flow images is obtained by the use of ultrasound contrast agents. These agents are micron-size gas bubbles that can navigate through the smallest capillaries without obstruction. However, free bubbles of such a small size dissolve quickly due to the osmotic diffusion of the gas inside. Contrast microbubbles are encapsulated by a few-nanometer-thick layer of lipids, proteins, or other surface-active materials that stabilizes them against premature dissolution. They are intravenously injected into a patient's body before imaging. The bubbles in the blood reflect more sound than the surrounding tissue and give a clear image of the myocardial perfusion (blood flow in the cardiac arteries) during contrast echocardiography.[1,2] The dynamics of these bubbles have been investigated by many researchers using *in vitro* ultrasound experiments[3–6] and models.[3,6–10]

Strong ultrasound pulses of large amplitude and higher power can destroy these bubbles by rupturing the encapsulation. Microbubble destruction may be useful in real-time blood flow velocity measurement,[11,12] stimulating arteriogenesis,[13] or targeted drug delivery.[14–16] In each application after microbubbles are intravenously injected, they are destroyed in a specific tissue region by an ultrasound pulse. After the loss of signal due to bubble destruction, from the time it takes for bubbles to show up in the region the blood velocity can be estimated. Song *et al.* found that destruction of these bubbles stimulates growth of new blood vessels in the region (arteriogenesis).[13] The bubbles can be functionalized so that it preferentially attaches to a target tissue, e.g., tumors, and then burst to destroy the tumor. They can also be coated with drugs and genes that can be released to the tumor upon destruction, without serious side effects. Shohet *et al.*[14] were able to deliver adenoviral transgene to rat myocardium through ultrasound-mediated microbubble destruction.

The destruction of a particular contrast agent depends on numerous factors such as exciting pulse, liquid temperature, hydrostatic pressure, or amount of dissolved gas in the blood. The destruction is studied by several researchers.[17–27] Two distinct mechanisms have been suggested for bubble destruction—slow gas diffusion and fast fragmentation. While varying the excitation, it was found that there is a threshold on the strength of the excitation that is needed for destruction. The threshold excitation was found to be different for different contrast agents due to the difference in the strength of the encapsulation as well as the solubility of the gas content in the surrounding liquid. Klibanov *et al.*[26] studied destruction of Albunex® and Optison® microbubbles and

[a)]Author to whom correspondence should be addressed. Electronic mail: sarkar@me.udel.edu

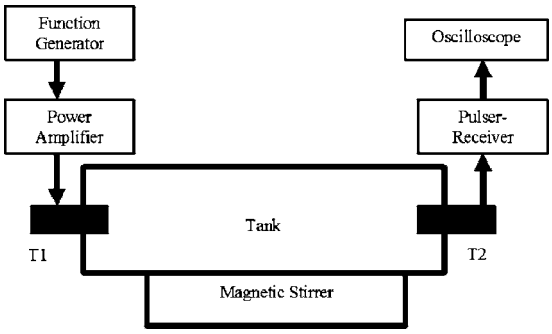

FIG. 1. Attenuation setup.

found that Albunex® is more prone to loss of echogenicity than is Optison®. They concluded that the gas inside plays a more important role than the shell, as Optison® has sparingly soluble perfluoropropane gas whereas Albunex® is air filled. Moran *et al.*[22] and Sonne *et al.*[11] however, observed that Optison® destruction rate is much faster than Definity® though they have a similar high-molecular-weight gas core. They ascribed this difference to the difference in shell composition—Definity® with a lipid layer showed more resistance as compared with albumin-coated Optison®. Shi *et al.*[21] observed that acoustic pressures causing microbubble destruction for one agent are usually not necessarily the same for another agent.

In this paper, we investigate the *in vitro* destruction of contrast agent Definity® (Bristol Myers-Squibb Imaging, North Ballerina, MA, USA). Definity® is a Food and Drug Administration (FDA)-approved contrast agent containing perfluoropropane gas surrounded by a lipid encapsulation. We measured the attenuation of ultrasound as a function of time under excitation with varying pulse repetition frequencies and amplitudes. The excitation affects the contrast microbubbles, giving rise to a change in attenuation over time. To our knowledge, the measurement of attenuation has not been used as a means to investigate bubble destruction in the past. In the following, we describe the experimental setup and discuss the results.

II. EXPERIMENTAL SETUP

The schematic of the attenuation setup is shown in Fig. 1. An unfocused broadband 5-MHz transducer mounted on the wall of a plastic tank was used as a transmitter. The −6 dB bandwidth for this transducer is 3.1–6.55 MHz, respectively, and its nominal aperture (D_0) is 12.5 mm. Another unfocused broadband transducer, with a center frequency of 3.5 MHz, was mounted on the opposite wall of the tank to act as a receiver. The receiver and the transmitter faced each other and were separated by a distance of 10.5 cm. The on-axis Rayleigh distance, given as $(D_0^2/4\lambda)$, for the transmitter is 13.02 cm ($\lambda = 0.3$ mm is the wavelength in water). However, Zemanek[28] and Blackstock[29] showed by a detailed computation of the near-field beam behavior that the indicated boundary of the near-field pattern is at $0.75D_0^2/4\lambda$ which in our case is 9.765 cm. The receiver therefore was in the far-field region. The beam divergence was checked to be minimal in this region.

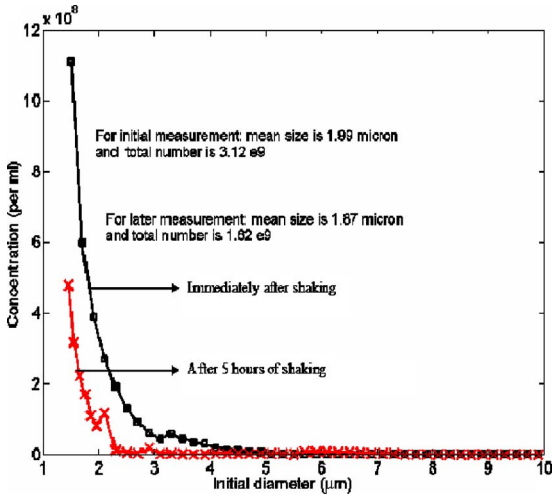

FIG. 2. Bubble size distribution at 2 times, immediately after shaking, and after 5 h.

We used a function generator (33250A, Agilent, Palo Alto, CA, USA) and a power amplifier (ENI A150, Rochester, NY, USA) (Fig. 1) to produce one-cycle bursts at selected PRFs and pressure amplitudes. The received signal, amplified by a Pulser-Receiver (5800PR, Panametrics, Waltham, MA, USA) was fed into an oscilloscope (TDS2012, Tektronix, OR, USA) and stored in a computer via General-Purpose Interface Board (GPIB) interface. Labview® (National Instruments, USA) controlled data acquisition and transfer. MATLAB® (Math-work Inc, Natick, MA, USA) was used for postprocessing the data. A 0.4-mm needle hydrophone (PZT-Z44-0400, Onda Corporation, CA, USA) was used to calibrate the transducers. For each set of parameters the experiment was repeated at least three times.

III. CONTRAST AGENT

Definity microbubbles are supplied in vials. Before they are administered to a patient, they are prepared following a specific protocol prescribed by the manufacturer. Following this protocol, the vial was shaken in a Vial-Mix™ (Bristol-Myers Squibb, North Ballerina, MA, USA) for 45 s. 2 min after shaking, the bubble suspension was injected in the tank containing a standard phosphate-based buffer, Isoton-II (Beckman Coulter, Florida, USA). The results reported here were obtained by diluting 16 μl of Definity in 400 ml of Isoton-II. Experiments were started 1 min after injection. A magnetic stirrer (Fisher Scientific) rotated the emulsion to produce a homogeneous microbubble solution. Experiments are performed at room temperature.

Size distribution

We measured the size distribution of microbubbles in a Definity sample using a Coulter Counter (Model Z-2, Beckman Coulter Instruments, FL, USA). The size distribution was measured immediately after the sample was prepared and also after 5 h. In the intervening period the sample is left undisturbed. Figure 2 shows that there is no significant change in the mean size of the bubble (1.99 and 1.87 μm,

respectively) though there is a reduction in the total number of bubbles from 3.12×10^9 to 1.62×10^9/ml. Definity microbubbles are reasonably stable even 5 h after preparation. Smaller bubbles with a larger surface-to-volume ratio seem to be less stable because of stronger diffusion.[30] Smaller bubbles do not contribute significantly to scattering, except when driven at a frequency close to resonance. The elastic effects of the encapsulation increase the resonance frequency of these microbubbles more than that of a free bubble of the same size.[5,7,9] Moreover, the enhancement of scattering at resonance is much less pronounced due to the stiff encapsulation of a contrast agent such as Definity. This, perhaps, explains the findings of Sboros *et al.*[31] that there was no significant change in scattering over time.

For comparison, we also measured the size distribution optically by using an Olympus BH-2 microscope in conjunction with a Canon MVC-300 digital camera. Photos were taken in light transmission mode [Fig. 3(a)]. Figure 3(b) shows that the size distributions measured optically and by the Coulter counter compare well with each other, providing credence to the reliability of the measuring procedure.

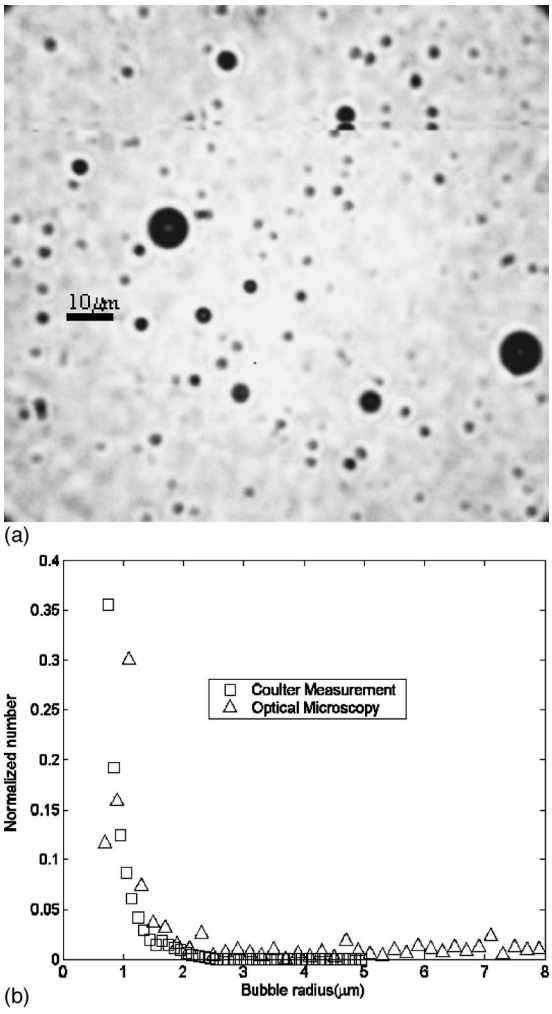

FIG. 3. (a) Optical image of Definity® under microscope; the bar indicates 10 μm. (b) Comparison of size distribution measurement using Coulter counter and optical microscope.

IV. METHOD

For the broadband pulse, one can assume that different frequency components travel as plane waves independent of each other and undergo dissipation:

$$P(x,t) = \mathrm{Re}\, P_0 e^{i\omega(t-x/c)} e^{-\alpha(\omega)/2x},$$
$$I(x) = |P(x,t)|^2 = I_0 e^{-\alpha(\omega)x}, \tag{1}$$

where Re indicates the real part, P_0 and I_0 are the incident pressure amplitude and intensity, respectively, c is the sound speed in the liquid, ω is the frequency, and $\alpha(\omega)$ is the attenuation at frequency ω per unit distance. Note that multiple scattering, coherent contribution,[32] and dispersion due to the presence of bubbles are neglected due to the extremely low void fraction of 5×10^{-7}. Commander and Prosperetti[33] estimate the speed of sound in a bubbly mixture as

$$V^2 \approx c^2/(1+\beta\rho c^2/p_\infty), \tag{2}$$

indicating a less than 1% variation in the sound speed. Indeed, by measuring the delay in pulse arrival in our setup in the presence of bubbles, we found that the speed is not varying significantly. Each bubble contributes to the attenuation of a particular frequency component according to its extinction cross-section $\sigma_e(a;\omega)$:

$$\alpha(\omega) = 10(\log_{10} e)N\int_{a_{\min}}^{a_{\max}} \sigma_e(a;\omega) f(a)\, da, \tag{3}$$

where $f(a)$ is the normalized number of bubbles per unit radius a and N is the number of bubbles per unit volume. Equation (3) indicates that the attenuation in this regime varies linearly with bubble density or concentration. Note that here the attenuation is independent of the excitation amplitude. From the measured data, the attenuation spectrum is computed:

$$\alpha(\omega) = 10\log_{10}\left(\frac{V_{\mathrm{ref}}^2(\omega)}{V_{\mathrm{sig}}^2(\omega)}\right)\Big/ d, \tag{4}$$

where $\alpha(\omega)$ is in dB/cm, d is the distance between the receiver and the transmitter, and $V_{\mathrm{ref}}(\omega)$ and $V_{\mathrm{sig}}(\omega)$ are the received sound in the absence and presence of contrast agents, respectively. Figure 4(a) shows that a typical original and attenuated (due to bubbles) signals in the time domain form a single experiment. The fast Fourier transform (FFT) of the time domain signals shown in Fig. 4(a) are shown in Fig. 4(b).

However, in this paper we used high-intensity ultrasound for initiating the destruction of microbubbles, which renders the bubble motion nonlinear, making the linear theory of propagation and attenuation described above inappropriate. We have recently investigated the pressure amplitude dependence of attenuation through Definity®, establishing the limits of linear theory. We found that the attenuation becomes dependent on pressure for pressure values above 0.26 MPa[34] (which is much lower than the excitation levels studied here). Computed $\alpha(\omega)$, nevertheless, is expected to give a measure of the decrease in the signal due to bubbles. From

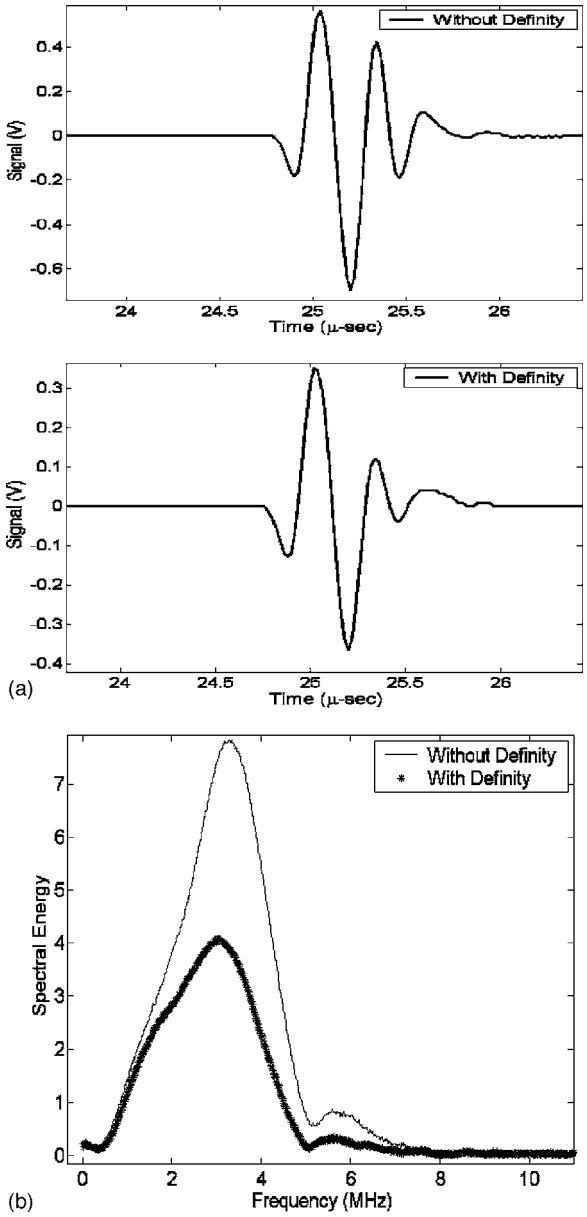

FIG. 4. (a) Signals with and without bubbles. (b) FFT of the signal at 0.78 MPa.

Fig. 4(a), it is evident that there is no significant nonlinear distortion in the wave and the condition of the weak shock is not reached over the given distance of travel.[35] However, there might be a redistribution of energy from one frequency to another. Therefore, rather than considering the frequency spectrum, we compute normalized attenuation (NA) with time. It is obtained by dividing attenuation $A(t)$ at any time by its initial value $A(0)$.

$$NA(t) = \frac{A(t)}{A(0)}; \quad A = 10 \log_{10}\left(\frac{\Sigma_{\omega} V^2_{\mathrm{ref}}(\omega)}{\Sigma_{\omega} V^2_{\mathrm{sig}}(\omega)}\right) \Big/ d. \qquad (5)$$

The total energy in the spectrum is considered instead of the individual frequency contribution [Eq. (4)].

V. RESULTS AND DISCUSSION

Strong acoustic excitation leads to the instability and destruction of microbubbles. Shi and Forsberg have shown that for Optison® bubbles, even before destruction, the attenuation spectrum changes with time.[36] They also observed a shift in the peak towards lower frequency in suggesting an increase in bubble size. It was attributed to the ingression of air into Optison®bubbles and the slow diffusion out of perfluorocarbon gas. However, the peak was observed to shift back at a later time and the attenuation decreased. We measured attenuation for various excitation amplitudes and PRFs and investigated bubble destruction as indicated by a decrease in attenuation with time. Under excitation, bubble destruction takes place in different ways, such as by slow outward diffusion of the gas, by rupture of the encapsulation and dissolution of the resulting free bubble, or through a catastrophic process of breaking up into smaller bubbles.[24] All of them results in decreased attenuation.

We performed the attenuation measurement using excitations with varying PRFs and pressure amplitudes. Figure 5(a) shows the variation of normalized attenuation with time when bubbles are subjected to acoustic excitation with a PRF of 50 Hz under different pressure amplitudes. Figures 5(b) and 5(c) show the same plots for 100 and 200 Hz, respectively. For the lowest pressure of 0.78 MPa, we find that the attenuation level increases with time for all three PRFs. With increased excitation levels, the attenuation decreases with time, indicating a deterioration of the bubble population. We find that there is a threshold pressure, above which the measured attenuation shows a decrease with time. For all three PRFs, it is around 1.2 MPa, even though one would expect that the critical pressure for destruction would be reduced with increasing PRF. Increasing the pressure amplitude beyond this critical value results in a faster decrease of attenuation indicating a faster rate of destruction. At each PRF the rate of destruction is very slow at pressure values slightly above the critical pressure. For such cases, the primary mode of destruction is gas dissolution.[19,20,24,25] The ultrasound excitation leads to a structural deterioration of the encapsulation, such as the appearance of small cracks, facilitating gas diffusion. For the highest-pressure levels (2.6 and 2.97 MPa), the attenuation curves tend to overlap, suggesting that the destruction becomes independent of pressure values. The attenuation does not show much dependence on PRF, as is evident from Fig. 6 except for intermediate excitation levels. The excitation-independent attenuation decrease indicates a complete rupture of the encapsulation. Note that nonlinear emission from the contrast agent under excitation has primarily been used in literature as a signature of bubble fragmentation, and, accordingly, excitation thresholds were determined. Measuring scattered response with increasing pressure levels, Chen *et al.*[27] determined an inertial cavitation threshold marked by a sudden increase in the frequency spectra between each pair of harmonics. They found fragmentation thresholds for Optison® (0.13 MPa at 1.1 MHz and 0.48 MPa at 3.5 MHz), Sonazoid (0.15 MPa at 1.1 MHz and 0.58 MPa at 3.5 MHz), bisphere 0.2*X* (0.19 MPa at 1.1 MHz and 0.73 MPa at 3.5 MHz) and bisphere 0.7*X*

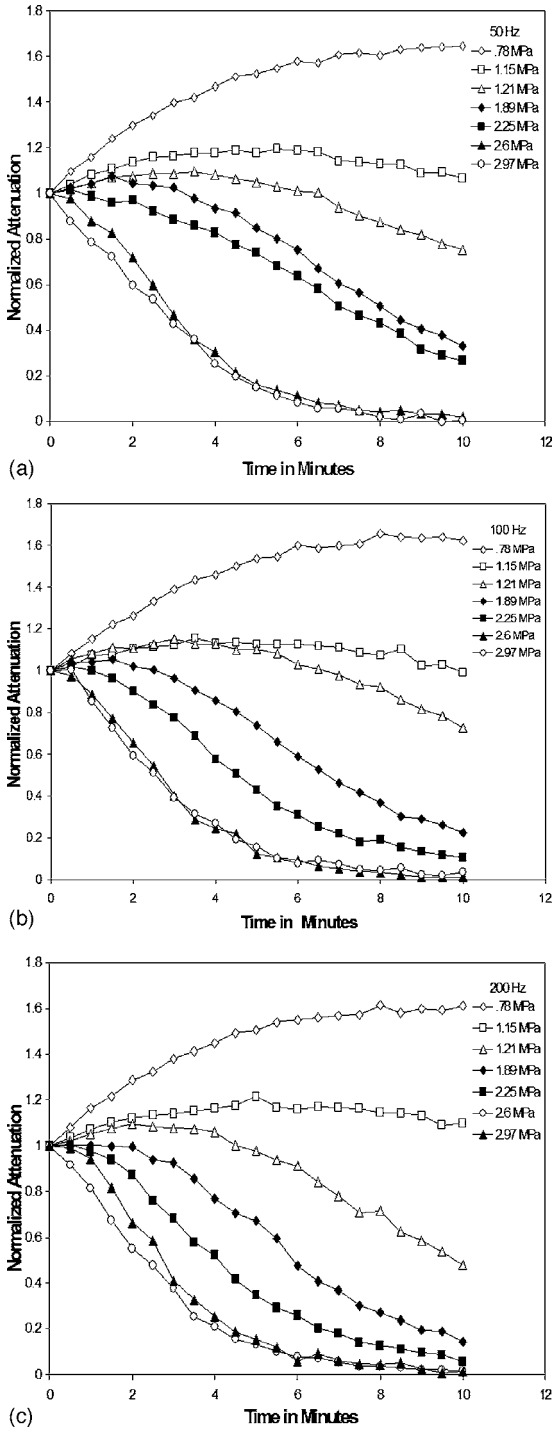

FIG. 5. Variation of normalized attenuation with time under different acoustic pressure amplitudes for PRF of (a) 50 Hz, (b) 100 Hz, and (c) 200 Hz.

(0.23 MPa at 1.1 MHz and 0.96 MPa at 3.5 MHz). Similarly, Sboros *et al.*[44] found a maximum in the second-harmonic normalized backscatter for Definity® at 0.5 MPa for 1.6-MHz driving frequency, and suggested a bubble destruction above such pressure. Note that our experiment is performed under single-cycle bursts form a 5-MHz transducer. The power delivered is lower at the higher frequency, which might explain our higher threshold value.

In Figs. 5(a)–5(c), we note that at lower-pressure amplitudes, the attenuation tends to increase with time, indicating a transient growth in the bubble radius. The bubble oscillation at low levels of excitation results in an increased permeability of the shell and a larger diffusion of gases. Definity® bubbles are made with perfluorocarbon gas inside. Initially, more air will diffuse in than heavy, less soluble perfluorocarbon gas diffuses out, as the time scale of diffusion of these two gases are different.[37,38] The increased bubble size will give rise to a larger attenuation. Over a longer period of time, the process, reversed, and the attenuation is reduced. For 0.78 MPa, we do not see the eventual decrease in the time scale of the experiment (10 min), but at a slightly higher-pressure amplitude of 1.15 MPa we observe it. In fact, for many cases the low- to intermediate-pressure amplitudes in Figs. 5(a)–5(c) display an initial increase followed by a final decrease. Over a longer period of time, the partial pressure of air inside the bubble reaches equilibrium with the dissolved air outside. The gas continues to slowly diffuse out and the bubble shrinks, leading to a reduced attenuation. Kabalnov *et al.*[37] presented a model of a multicomponent microbubble dissolution that showed such initial swelling of microbubble over a very short time scale. However, the model did not account for the permeability of the encapsulation, which would delay the process. A transient increase in bubble size due to gas diffusion was also reported by Guan and Matula, where they determined the instantaneous bubble size by light scattering.[39] However, in the present setup an increase in attenuation can be caused by other effects such as accumulation of bubbles in the acoustic beam due to radiation pressure. In the following, we briefly consider this effect.

A. Bubble motion due to radiation pressure

The governing equation for the translatory motion of a bubble of radius $R(t)$ in an acoustic field can be described by the force balance:[40,41]

$$\bar{F}_M = \bar{F}_B + \bar{F}_D, \quad \bar{F}_M = \tfrac{1}{2}\rho\langle V(t)\rangle_T \bar{\nu}, \quad \bar{F}_B = -\langle \nabla P_A(t) V(t)\rangle_T,$$
$$\bar{F}_D = (\beta_1\langle R(t)\rangle_T + \beta_2\langle R(t)\rangle_T^2 \|\bar{\nu}\|)\bar{\nu}, \tag{6}$$

where $\bar{F}_M$, $\bar{F}_B$, and $\bar{F}_D$ are the added mass force, Bjerknes force, and drag force, respectively. $V(t)$ refers to the instantaneous bubble volume, $P_A(t)$ is the acoustic pressure, ρ is the liquid density, $\bar{\nu}$ denotes the bubble translation velocity and β_1 and β_2 are constants with values of 0.015 $\mathrm{Ns/m^2}$ and 4000 $\mathrm{Ns^2/m^3}$, respectively.[40,41] For the void fraction of $\beta = 5.15\times10^{-7}$ the average bubble-bubble separation is 250 times its radius (using the mean diameter of 1.99 μm). The secondary Bjerknes force arising from bubble-bubble interactions becomes negligible at this separation.[42,43] The bubble radius and the volume in Eq. (6) can be computed using bubble dynamics; the radial oscillation of a bubble is described by a Rayleigh-Plesset-type equation. There are various models for the encapsulation. We have developed an interfacial rheological model[9,10] that leads to the following equation for the bubble radius R:

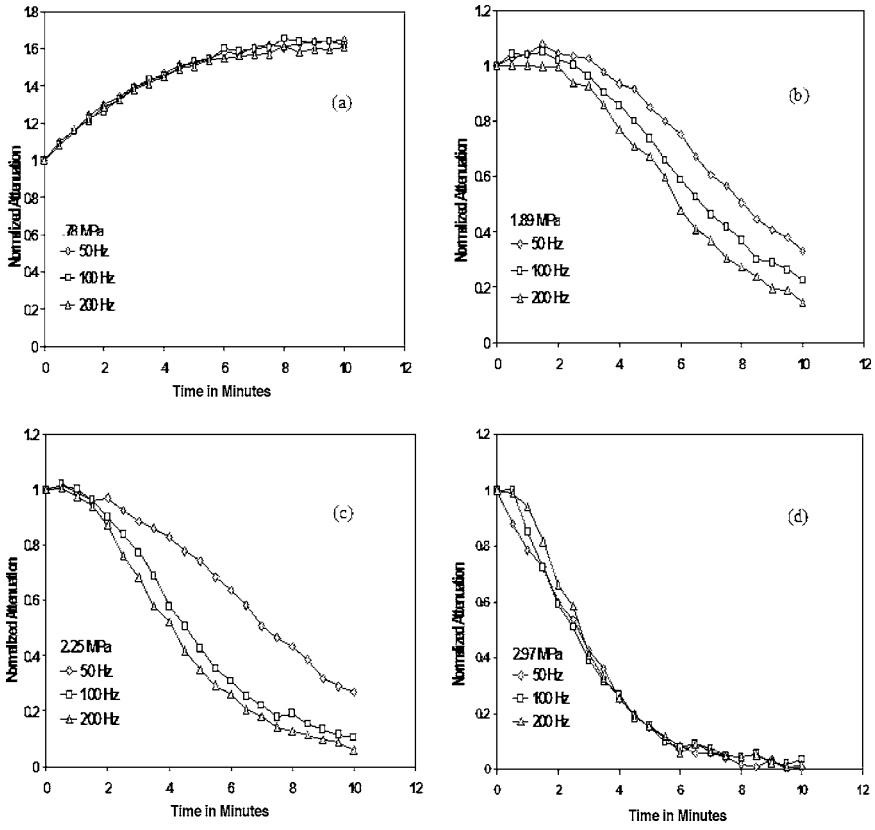

FIG. 6. Normalized attenuation with time under different PRFs at four different pressure amplitudes: (a) 0.78 MPa, (b) 1.89 MPa, (c) 2.25 MPa, and (d) 2.97 MPa.

$$\rho\left(R\ddot{R}+\frac{3}{2}\dot{R}^2\right)=P_{G_0}\left(\frac{R_0}{R}\right)^{3k}-4\mu\frac{\dot{R}}{R}-\frac{2\gamma}{R}-\frac{4\kappa^s\dot{R}}{R^2}-P_0+P_A\sin\omega t, \tag{7}$$

where, R_0 is the initial bubble radius, ρ and μ are liquid density and viscosity, P_{G_0} is the initial gas pressure, P_0 is the hydrostatic pressure and $P_A \sin \omega t$ represents the acoustic excitation. The encapsulation is modeled by the interfacial rheological properties surface tension γ and surface dilatational viscosity κ^s. The encapsulation parameters are determined by matching with the measured attenuation data; $\gamma = 1.47$ N/m and $\kappa^s = 1.93 \times 10^{-3}$ m s P. The pressure gradient is obtained by measuring the pressure across the acoustic beam. Using Eq. (6) we determine the velocity of a bubble at the edge of the beam and thereby its motion by time integration. We find that at an excitation pressure of 0.78 MPa, a bubble moves 3.01 nm in one cycle. Therefore, for the extremely low duty cycle (0.001%, 0.002%, and 0.004% corresponding to 50, 100, and 200-Hz PRF, respectively) the bubble movement is not sufficient for the agglomeration or development of spatial inhomogeneity, at least in a short time. The increase in attenuation is seen even for early times (Fig. 5) before any accumulation can take place. Furthermore, the slow rotation of the magnetic stirrer ensured the maintenance of a nearly homogeneous emulsion.

B. Modes of destruction and time scale

Our study suggests that there are three distinct bubble behaviors—bubble growth at low pressures, amplitude-dependent destruction at intermediate pressures (higher than 1.2 MPa), and destruction independent of amplitude at high pressures. Attenuation shows a very weak dependence on the PRF. At higher pressure and later times the curves tend to overlap. At these pressure values the destruction is dominated by shell rupture.

The variation of normalized attenuation data with time is expressed by an exponential curve:

$$A(t) = A(0)\exp(-mt). \tag{8}$$

Here, m, the decay constant, is a function of the intensity of excitation ($\sim P_A{}^2$) and the PRF. We obtained the decay constant (m) by fitting an exponential to the data set in Figs. 5(a)–5(c), taking only the descending part of the curves. Table I shows the values of m under different excitation pressures and PRFs. m increases with P_A. At the PRF of 200 Hz the destruction become independent of pressure above 2.25 MPa. The variation of m with P_A is shown in Fig. 7 for different PRFs. m varies as $P_A{}^{1.8}$, $P_A{}^{2.0}$, and $P_A{}^{1.4}$ for PRF of 50, 100, and 200 Hz, respectively. It should be noted that

TABLE I. Values of decay constant m (min^{-1}) for different pressure amplitudes and PRFs.

Pressure in MPa	50 Hz	100 Hz	200 Hz
1.21	0.1	0.08	0.14
1.89	0.17	0.21	0.25
2.25	0.17	0.28	0.32
2.6	0.41	0.50	0.43
2.97	0.49	0.41	0.47

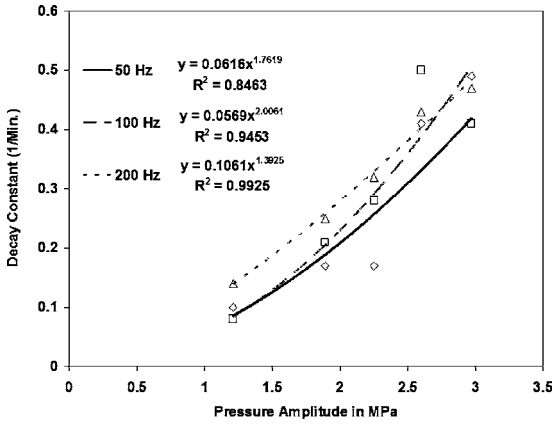

FIG. 7. Variation of decay constant $m(\min^{-1})$ with pressure amplitudes for varying PRFs.

from a simple total-energy consideration, one would expect m to be a function of ${P_A}^{2}*$ PRF. However, note that the destruction is a combined effect of gas diffusion and shell rupture at larger pressure values, and it is not just the total acoustic energy delivered that might explain the deviation.

VI. SUMMARY

We have investigated the destruction of contrast microbubbles under acoustic excitation, taking the Definity® microbubble as a test case. These are $1-2$-μm bubbles stabilized by a lipid encapsulation. We measure the attenuation of ultrasound through a solution of Definity® as a function of time at various pressure amplitudes and PRFs. For smaller pressure amplitudes (e.g., 0.78 MPa) we obtain an increase in attenuation with time, indicating bubble growth due to gas diffusion. There is a critical pressure level above which attenuation tends to decrease with time, indicating bubble dissolution. The critical pressure level is $\sim$1.2 MPa for all three PRFs (50, 100, and 200 Hz) considered here. The rate of destruction increases with increase in pressure amplitude, suggesting a slow mechanism of gas diffusion. In contrast, at very high pressures the process becomes independent of excitation amplitudes and the steep decay indicates a faster destruction mode by shell rupture. The destruction shows only a weak dependence on PRF. We also fitted an exponential decay curve for the decay in attenuation. The decay constant m varies as ${P_A}^{1.8}$, ${P_A}^{2.0}$, and ${P_A}^{1.4}$ for PRF of 50, 100, and 200 Hz, respectively.

The ultrasound-mediated transient bubble growth below critical pressure would help achieve an enhanced scattering in an ultrasound-activated contrast imaging. In this mode, a second activating pulse could be used to induce bubble growth shortly before the imaging pulse is sent to obtain enhanced scattering signals from activated contrast bubbles. The saturation in bubble breakup at higher-pressure amplitudes (decreased attenuation being independent of pressure amplitude) indicates that one need not use any higher strength for inducing destruction, which might cause damage to the surrounding tissue. Further *in vivo* research is needed to establish optimum operational ranges for different clinical applications.

ACKNOWLEDGMENTS

K.S. acknowledges the DOD contract (DAMD17-03-1-0119), the NSF contract (CTS-0352829), and the University of Delaware Research Foundation. We thank Professor Ulhas Naik and Dr. Sai for helping us with the Coulter Counter and Dr. Arup Nandi for helping us with the microscope.

[1] *Ultrasound Contrast Agents: Basic Principles and Clinical Applications*, 2nd ed., edited by B. B. Goldberg, J. S. Raichlen, and F. Forsberg (Martin Dunitz, London, 2001).
[2] P. J. A. Frinking, A. Boukaz, J. Kirkhorn, F. J. Ten Cate, and N. de Jong, "Ultrasound contrast imaging: Current and new potential methods," Ultrasound Med. Biol. **26**, 965 (2000).
[3] P. J. A. Frinking and N. de Jong, "Acoustic modeling of shell-encapsulated gas bubbles," Ultrasound Med. Biol. **24**, 523 (1998).
[4] W. T. Shi, F. Forsberg, A. L. Hall, R. Y. Chiao, J. Liu, S. Miller, K. E. Thomenius, M. A. Wheatley, and B. B. Goldberg, "Subharmonic imaging with microbubble contrast agents: Initial results," Ultrason. Imaging **21**, 79 (1999).
[5] L. Hoff, P. C. Sontum, and J. M. Hovem, "Oscillations of polymeric microbubbles: Effect of the encapsulating shell," J. Acoust. Soc. Am. **107**, 2272 (2000).
[6] K. E. Morgan, J. S. Allen, P. A. Dayton, J. E. Chomas, A. L. Klibanov, and K. W. Ferrara, "Experimental and theoretical evaluation of microbubble behavior: Effect of transmitted phase and bubble size," IEEE Trans. Ultrason. Ferroelectr. Freq. Control **47**, 1494 (2000).
[7] C. C. Church, "The effects of an elastic solid surface layer on the radial pulsations of gas bubbles," J. Acoust. Soc. Am. **97**, 1510 (1995).
[8] D. B. Khismatullin and A. Nadim, "Radial oscillations of encapsulated microbubbles in viscoelastic liquids," Phys. Fluids **14**, 3534 (2002).
[9] D. Chatterjee and K. Sarkar, "A Newtoninan rheological model for the interface of microbubble contrast agents," Ultrasound Med. Biol. **29**, 1749 (2003).
[10] K. Sarkar, W. T. Shi, D. Chatterjee, and F. Forsberg, "Characterization of ultrasound contrast microbubbles using *in vitro* experiments and viscous and viscoelastic interface models for encapsulation," J. Acoust. Soc. Am. **118**, 539 (2005).
[11] C. Sonne, F. Xie, J. Lof, J. Oberdorfer, P. Phillips, E. C. Everbach, and T. R. Porter, "Differences in Definity and Optison microbubble destruction rates at a similar mechanical index with different real-time perfusion systems," J. Am. Soc. Echocardiogr **16**, 1178 (2003).
[12] T. R. Porter, F. Xie, M. Silver, D. Kricsfeld, and E. O'Leary, "Real-time perfusion imaging with low mechanical index pulse inversion Doppler imaging," J. Am. Coll. Cardiol. **37**, 748 (2001).
[13] J. Song, M. Qi, S. Kaul, and R. J. Price, "Stimulation of arteriogenesis in skeletal muscles by microbubble destruction with ultrasound," Circulation **106**, 1550 (2002).
[14] R. V. Shohet, S. Chen, Y. T. Zhou, Z. W. Wang, R. S. Meidell, T. H. Unger, and P. A. Grayburn, "Echocardiographic destruction of albumin microbubbles directs gene delivery to the myocardium," Circulation **101**, 2554 (2000).
[15] R. J. Price, D. M. Skyba, S. Kaul, and T. C. Skalak, "Delivery of colloidal particles and red cells to tissue through microvessel ruptures created by targeted microbubble destruction with ultrasound," Circulation **98**, 1264 (1998).
[16] T. R. Porter, P. L. Iversen, S. Li, and F. Xie, "Interaction of diagnostic ultrasound with synthetic oligonucleotide-labeled perfluorocarbon-exposed sonicated dextrose albumin microbubbles," J. Ultrasound Med. **15**, 577 (1996).
[17] T. R. Porter and F. Xie, "Transient myocardial contrast after initial exposure to diagnostic ultrasound pressures with minute doses of intravenously injected microbubbles," Circulation **92**, 2391 (1995).
[18] K. W. Walker, G. A. Pantely, and D. J. Sahn, "Ultrasound-mediated destruction of contrast agents: Effect of ultrasound intensity, exposure and frequency," Invest. Radiol. **32**, 728 (1997).
[19] A. L. Klibanov, K. W. Ferrara, M. S. Hughes, J. H. Wible, J. K. Wojdyla, P. A. Dayton, K. E. Morgan, and G. H. Brandenburger, "Direct videomicroscopic observation of the dynamic effects of medical ultrasound on ultrasound contrast microspheres," Invest. Radiol. **33**, 863 (1998).
[20] P. A. Dayton, K. E. Morgan, A. L. Klibanov, G. H. Brandenburger, and K. W. Ferrara, "Optical and acoustical observations of the effects of

ultrasound on contrast agents," IEEE Trans. Ultrason. Ferroelectr. Freq. Control **46**, 220 (1999).
[21] W. T. Shi, F. Forsberg, A. Tornes, J. Østensen, and B. B. Goldberg, "Destruction of contrast microbubbles and the association with inertial cavitation," Ultrasound Med. Biol. **26**, 1009 (2000).
[22] C. M. Moran, T. Anderson, S. D. Pye, V. Sboros, and W. N. Mcdicken, "Quantification of microbubble destruction of three fluorocarbon-filled ultrasonic contrast agents," Ultrasound Med. Biol. **26**, 629 (2000).
[23] V. Sboros, C. M. Moran, D. Pye, and W. N. Mcdicken, "Contrast agent stability: A continuous B-mode imaging approach," Ultrasound Med. Biol. **27**, 1367 (2001).
[24] J. E. Chomas, P. A. Dayton, D. May, J. Allen, A. L. Klibanov, and K. W. Ferrara, "Optical observation of contrast agent destruction," Appl. Phys. Lett. **77**, 1056 (2000).
[25] J. E. Chomas, P. Dayton, J. Allen, K. Morgan, and K. W. Ferrara, "Mechanisms of contrast agent destruction," IEEE Trans. Ultrason. Ferroelectr. Freq. Control **48**, 232 (2001).
[26] A. L. Klibanov, M. S. Hughes, J. K. Wojdyla, J. H. Wible, Jr., and G. H. Brandenburger, "Destruction of contrast agent microbubbles in the ultrasonic field: The fate of the microbubble shell and the importance of the bubble gas content," Acad. Radiol. **9**, S41 (2002).
[27] W. S. Chen, T. J. Matula, A. A. Brayman, and L. A. Crum, "A comparison of the fragmentation thresholds and inertial cavitation doses of different ultrasound contrast agents," J. Acoust. Soc. Am. **113**, 643 (2003).
[28] J. Zemanek, "Beam behavior within the nearfield of a vibrating piston," J. Acoust. Soc. Am. **49**, 181 (1971).
[29] D. T. Blackstock, *Fundamentals of Physical Acoustics* (Wiley, New York, 2000), p. 455.
[30] P. S. Epstein and M. S. Plesset, "On the stability of gas bubbles in liquid-gas solutions," J. Chem. Phys. **18**, 1505 (1950).
[31] V. Sboros, C. M. Moran, T. Anderson, and W. N. Mcdicken, "An *in vitro* comparison of ultrasonic contrast agents in solutions with varying air levels," Ultrasound Med. Biol. **26**, 807 (2000).
[32] K. Sarkar and A. Prosperetti, "Coherent and incoherent scattering by oceanic bubbles," J. Acoust. Soc. Am. **96**, 332 (1994).
[33] K. W. Commander and A. Prosperetti, "Linear pressure waves in bubbly liquids: Comparison between theory and experiments," J. Acoust. Soc. Am. **85**, 732 (1989).
[34] D. Chatterjee, K. Sarkar, P. Jain, and N. E. Chreppler, "On the suitability of broadband attenuation measurement for characterizing contrast microbubbles," Ultrasound Med. Biol. **31**, 781 (2004).
[35] O. V. Rudenko and S. I. Soluyan, *Theoretical Foundation of Nonlinear Acoustics* (Plenum, New York, 1977).
[36] W. T. Shi and F. Forsberg, "Ultrasonic characterization of nonlinear properties of contrast microbubbles," Ultrasound Med. Biol. **26**, 93 (2000).
[37] A. Kabalnov, D. Klein, T. Pelura, E. Schutt, and J. Weers, "Dissolution of multicomponent microbubbles in the bloodstream. I. Theory," Ultrasound Med. Biol. **24**, 739 (1998).
[38] A. Kabalnov, J. Bradley, S. Flaim, and D. Klein "Dissolution of multicomponent microbubbles in the bloodstream. II. Experiment," Ultrasound Med. Biol. **24**, 751 (1998).
[39] J. Guan and T. J. Matula, "Using light scattering to measure the response of individual ultrasound contrast microbubbles subjected to pulsed ultrasound *in vitro*," J. Acoust. Soc. Am. **113**, 643 (2004).
[40] D. Chatterjee and V. H. Arakeri, "Some investigations on the use of ultrasonics in travelling bubble cavitation control," J. Fluid Mech. **504**, 365 (2004).
[41] U. Parlitz, R. Mettin, S. Luther, I. Akhatov, M. Voss, and W. Lauterborn, "Spatiotemporal dynamics of acoustic cavitation bubble clouds," Philos. Trans. R. Soc. London, Ser. A **357**, 313 (1999).
[42] J. J. Rychak, A. L. Klibanov, and J. A. Hossack, "Acoustic radiation force enhances targeted delivery of ultrasound contrast microbubbles: *In vitro* verification," IEEE Trans. Ultrason. Ferroelectr. Freq. Control **52**, 421 (2005).
[43] P. A. Dayton, J. S. Allen, and K. W. Ferrara, "The magnitude of radiation force on ultrasound contrast agents," J. Acoust. Soc. Am. **112**, 2183 (2002).
[44] V. Sboros, C. M. Moran, T. Anderson, and W. N. Mcdicken, "An *in vitro* study of a microbubble contrast agent using clinical ultrasound imaging system," Phys. Med. Biol. **49**, 159 (2004).